Geochemistry, Geophysics, Geosystems®

AGU ADVANCING EARTH AND SPACE SCIENCE

RESEARCH ARTICLE
10.1029/2022GC010534

Key Points:

- Structural, geophysical, and geochemical investigations elucidate the structure and present volcanic activity of the Astroni Volcano
- We indicate the locations where we first detected hydrothermal emissions and temperature anomalies
- Resistivity anomalies and identified structural lineaments suggest the presence of active structures within the Astroni Volcano

Correspondence to:
R. Isaia,
roberto.isaia@ingv.it

Citation:
Isaia, R., Di Giuseppe, M. G., Troiano, A., Avino, R., Caliro, S., Santi, A., & Vitale, S. (2022). Structure and present state of the Astroni Volcano in the Campi Flegrei caldera in Italy based on multidisciplinary investigations. *Geochemistry, Geophysics, Geosystems*, *23*, e2022GC010534. https://doi.org/10.1029/2022GC010534

Received 25 MAY 2022
Accepted 17 NOV 2022

Author Contributions:
Conceptualization: Roberto Isaia, Maria Giulia Di Giuseppe, Antonio Troiano, Rosario Avino, Stefano Caliro, Alessandro Santi, Stefano Vitale
Data curation: Roberto Isaia, Maria Giulia Di Giuseppe, Antonio Troiano, Rosario Avino, Stefano Caliro, Alessandro Santi, Stefano Vitale
Formal analysis: Roberto Isaia, Maria Giulia Di Giuseppe, Antonio Troiano, Rosario Avino, Stefano Caliro, Alessandro Santi, Stefano Vitale
Funding acquisition: Roberto Isaia, Maria Giulia Di Giuseppe
Investigation: Roberto Isaia, Maria Giulia Di Giuseppe, Antonio Troiano,

Structure and Present State of the Astroni Volcano in the Campi Flegrei Caldera in Italy Based on Multidisciplinary Investigations

Roberto Isaia[1], Maria Giulia Di Giuseppe[1], Antonio Troiano[1], Rosario Avino[1], Stefano Caliro[1], Alessandro Santi[1], and Stefano Vitale[1,2]

[1]Istituto Nazionale di Geofisica e Vulcanologia, Osservatorio Vesuviano, Naples, Italy, [2]Dipartimento di Scienze della Terra, dell'Ambiente e delle Risorse (DiSTAR), Università degli Studi di Napoli Federico II, Naples, Italy

Abstract Despite its known reconstructed volcanic history, the structural setting and present state of the Astroni Volcano of the Campi Flegrei caldera in Italy are still poorly defined. Through structural, geophysical, and geochemical investigations, we elucidate the structure and present volcanic activity of the Astroni Volcano, which hosts tuff cones, scoriae cones, lava domes, and lakes on the crater floor. A volcano-tectonic analysis focused on the entire volcano edifice, coupled with electrical resistivity tomography of the shallower part of the Astroni crater, revealed the main rock formations, faults, and possible fluid patterns within the first 150 m depth. Two main NE–SW and NW–SE trending fault sets were imaged using electrical resistivity modeling and measurements along the wall of the volcanic edifice; they likely delimit a maar-like structure resulting from the highest energetic subplinian Astroni 6 eruption event and acted as magma pathways during the late eruptive activity stage. A 3D view of the reconstructed resistivity model revealed both deep root-conduit-like structures and shallower dome-like shapes for volcanic edifices on the crater floor. Gas and carbon compositions in the NNE sectors of the Astroni Lago Grande are similar to those of the Solfatara fumarole fluids, suggesting common hydrothermal origin and a possible link with a deep hydrothermal reservoir. This fluid-emission area along the border of the younger volcanic structure exhibits a +40°C maximum soil-temperature anomaly. The proposed volcano-tectonic architecture should improve the unrest scenarios in case of reactivation in this Campi Flegrei caldera sector and the monitoring strategies for the Astroni Volcano.

Plain Language Summary The Campi Flegrei caldera (Southern Italy) is one of the most productive explosive volcanic systems worldwide. The central-eastern sector of the caldera has recently been the location of several major volcanic vents, including the Astroni Volcano. It is very close to the Solfatara-Pisciarelli area, where the most significant energy release and largest variation of the volcanic and seismic activities characterize the ongoing unrest crisis of the Campi Flegrei. In this study, we aim to provide new insights regarding the structure of the Astroni Volcano and elucidate the present volcanic activity through a multidisciplinary approach that merges volcanological, structural, geophysical, and geochemical data. A volcano-tectonic analysis, coupled with a 3D electrical resistivity tomography, allowed us to define in detail the relation between the volcano-tectonic structures, rock bodies, and fluid circulation within the first 150 m depth of the Astroni crater. We describe for the first time the hydrothermal emission activity and thermal anomaly within the Astroni crater and suggest the possible involvement of the geothermal reservoir. These results will help better evaluate the unrest scenarios in case of reactivation in this Campi Flegrei caldera sector and implement effective monitoring strategies for the Astroni Volcano.

1. Introduction

Volcanic calderas generally host heterogeneous structures composed of several distinct eruptive centers, including lava domes, tuff rings and tuff cones of different ages and sizes (Acocella et al., 2015; Martì et al., 2008). Consequently, the reconstruction of the past activity of every eruptive center, as well as their depositional and volcano-tectonic setting, is highly important regarding the global understanding of caldera evolution. Usually, major deformation structures—such as eruptive fissures, faults, and related damage zones—formed during volcano-tectonic activity, which may have been characterized by caldera collapses (Acocella, 2007; Geyer & Martì, 2014) and may strongly control intracaldera volcanism (Rosi & Sbrana, 1987; Vitale & Isaia, 2014). Such arrays of structures also determine the formation and geometry of the caldera plumbing system and can act as

Rosario Avino, Stefano Caliro, Alessandro Santi, Stefano Vitale
Supervision: Roberto Isaia, Maria Giulia Di Giuseppe
Validation: Roberto Isaia, Maria Giulia Di Giuseppe, Antonio Troiano, Stefano Vitale
Visualization: Roberto Isaia, Maria Giulia Di Giuseppe, Antonio Troiano, Rosario Avino, Stefano Caliro, Alessandro Santi, Stefano Vitale
Writing – review & editing: Roberto Isaia, Maria Giulia Di Giuseppe, Antonio Troiano, Rosario Avino, Stefano Caliro, Alessandro Santi, Stefano Vitale

preferred pathways for magma flow. Furthermore, eruptive vent locations and their type of volcanism are strictly linked to the reactivation of such structures, as well as to the possible initiation of new eruptive events and/or the creation of shallow hydrothermal systems and fumarolic fields inside or close to the volcanic edifice (Gottsmann et al., 2007). The monitoring of such active structures is fundamental during periods of unrest at calderas because of their capacity to transfer signals of volcanic anomalies from certain depths to the surface, thereby indicating the possibility of escalation (Kennedy et al., 2018; Padron et al., 2012; Sabbarese et al., 2020). Hence, a multidisciplinary approach that provides volcanological, structural, geophysical, and geochemical constraints is essential for defining the current activity of a volcano and evaluating its hazard potential, especially in calderas with uncertain vent opening locations.

One of the best places to observe and investigate this close relation between structures and volcano-tectonic activity is the Campi Flegrei caldera in Southern Italy (Figure 1a), which is the most urbanized caldera in the world and has recently been the site of many vents active in its central-eastern sector (Bevilacqua et al., 2016; Di Vito et al., 1999; Orsi et al., 2004; Smith et al., 2011). Between 5.5 and 3.8 ka, at least 21 eruptions occurred, forming several volcanic edifices, including the tuff ring of the Astroni Volcano (Figure 1b), which formed at the edge of the minor Agnano caldera (Isaia et al., 2009; Vitale & Isaia, 2014) during a complex eruptive history characterized by at least seven distinct eruptions (Isaia et al., 2004). Although the volcanic and magmatic history of the Astroni Volcano has been reconstructed (Isaia et al., 2004; Tonarini et al., 2009), the structural architecture at depth and the present state of the volcano are still poorly understood. In the last few years, high-resolution imaging of the Campi Flegrei caldera's eruptive and deformation structures has become available, mainly through electric (Byrdina et al., 2014; Di Giuseppe et al., 2015; Di Giuseppe, Troiano, Di Vito, et al., 2017; Di Giuseppe & Troiano, 2019; Gresse et al., 2017; Isaia et al., 2015, 2021; Troiano et al., 2019, 2021; Vitale et al., 2019), electromagnetic (Siniscalchi et al., 2019; Troiano et al., 2014), gravimetric (Capuano et al., 2013; Young et al., 2020), and seismic (Battaglia et al., 2008; Calò & Tramelli, 2018; De Siena et al., 2010, 2017) surveys. However, these studies mainly focused on the most active parts of the Campi Flegrei caldera (i.e., the Solfatara and Pisciarelli areas and the Agnano Plain; Figure 1a). The only information about the Astroni Volcano structure is derived from large-scale geophysical surveys (e.g., across the entire Campi Flegrei caldera).

In this study, we aim to provide new insights regarding the structure of the Astroni Volcano and elucidate the present volcanic activity by means of a multidisciplinary approach that merges volcanological, structural, geophysical, and geochemical data. The study area is particularly interesting because of its volcanological history, which is characterized by several eruptions that occurred spatially and temporally close to one another, fed by magmas stalling at different depths and capable of reaching the surface within a few days (Astbury et al., 2018; Stock et al., 2016). We also aim to define in detail the relation between the volcano-tectonic structures, rock bodies, and fluid circulation in a recent volcano localized within the caldera sector, where the probability of a new vent opening is especially high (Bevilacqua et al., 2015; Orsi et al., 2004). Finally, we describe for the first time the hydrothermal emission activity and thermal anomaly within the Astroni crater and suggest the possible involvement of the geothermal reservoir that has been detected by geophysical surveys (e.g., Young et al., 2020), also due to the present unrest crisis at Campi Flegrei caldera.

2. Geological Setting and Volcanological Evolution of the Astroni Volcano

The Campi Flegrei caldera (Figure 1a) has been the site of approximately 70 eruptions since the last major collapse that occurred during the 15 ka Neapolitan Yellow Tuff (NYT) eruption. Most of the eruptions occurred in the central-eastern sector, including two Plinian events (Di Vito et al., 1999), among which the Agnano-Monte Spina (AMS) eruption (i.e., 4.5 ka; de Vita et al., 1999; Smith et al., 2011) also generated a small caldera, corresponding to the present Agnano Plain (Figure 1a). The AMS caldera collapse affected the pre-existing volcanic edifices, while its shape was strongly controlled by the reactivation of major faults defined by the regional NW–SE and NE–SW directions (Isaia et al., 2009). This fault array and related damage zones seem to favor the ascent of magmas or magmatic fluids, as observed in the Solfatara and Pisciarelli areas (Isaia et al., 2015, 2021; Troiano et al., 2019, 2021). More recent and subordinate E–W/ENE–WSW-and N–S/NNE–SSW-striking structures have also been observed between the Solfatara and Astroni volcanoes (Battaglia et al., 2008; Isaia et al., 2015, 2021; Vitale & Isaia, 2014). After the Agnano Plain collapse, volcanism occurred along its western margin, starting with a cluster of low-energy explosive eruptions and lava domes (i.e., Accademia-Solfatara area; Figure 1a) (Isaia

10.1029/2022GC010534

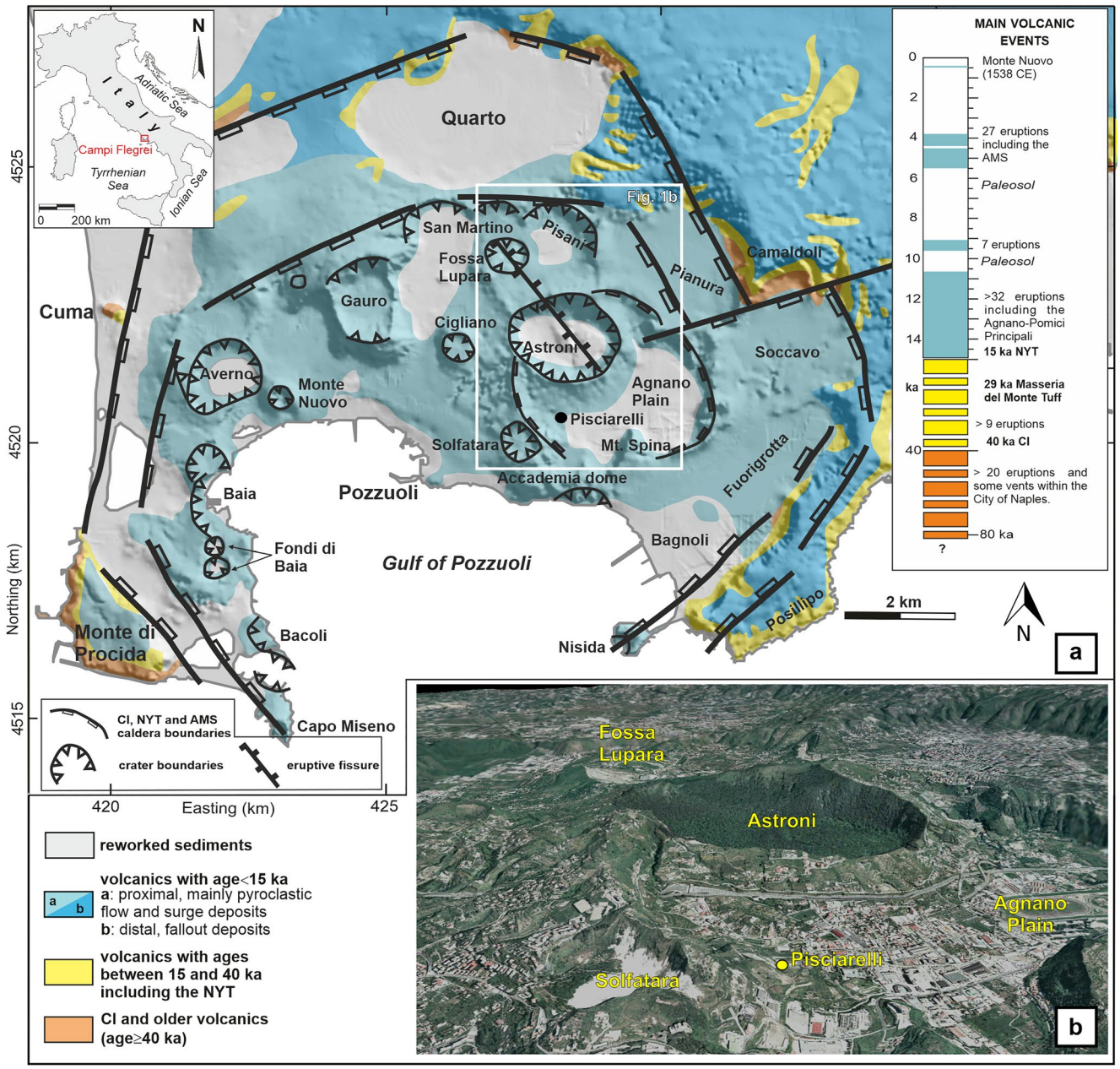

Figure 1. (a) Simplified geological map of Campi Flegrei modified after Troiano et al., 2019. CI: Campanian Ignimbrite; NYT: Neapolitan Yellow Tuff; AMS: Agnano-Monte Spina. (b) Satellite image of the Astroni-Solfatara sector.

et al., 2009, 2015). These events were shortly followed by multiple eruptions a few hundred meters northward, which formed the Astroni and Fossa Lupara volcanoes (Figures 1a and 1b).

The Astroni Volcano formed at the northwestern corner of the Agnano caldera (Figure 1a) due to seven explosive eruptions (labeled as Astroni 1–7). These eruptions emitted approximately 0.5 km^3 magma (Isaia et al., 2004) and formed a large tuff ring with approximately 2 km diameter. Volcanic activity was fed by trachytic to phonolitic magmas (Smith et al., 2011; Tonarini et al., 2009), likely due to separate magma bodies located at different depths (Astbury et al., 2018). An evolved shallow (i.e., at ~3.5 km depth) magma chamber has been recharged by a less evolved magma located deeper (i.e., at ~7.0 km depth) (Stock et al., 2018). The mixing of these two magmas occurred in the shallow magma system during a single recharge event; this event likely occurred between about

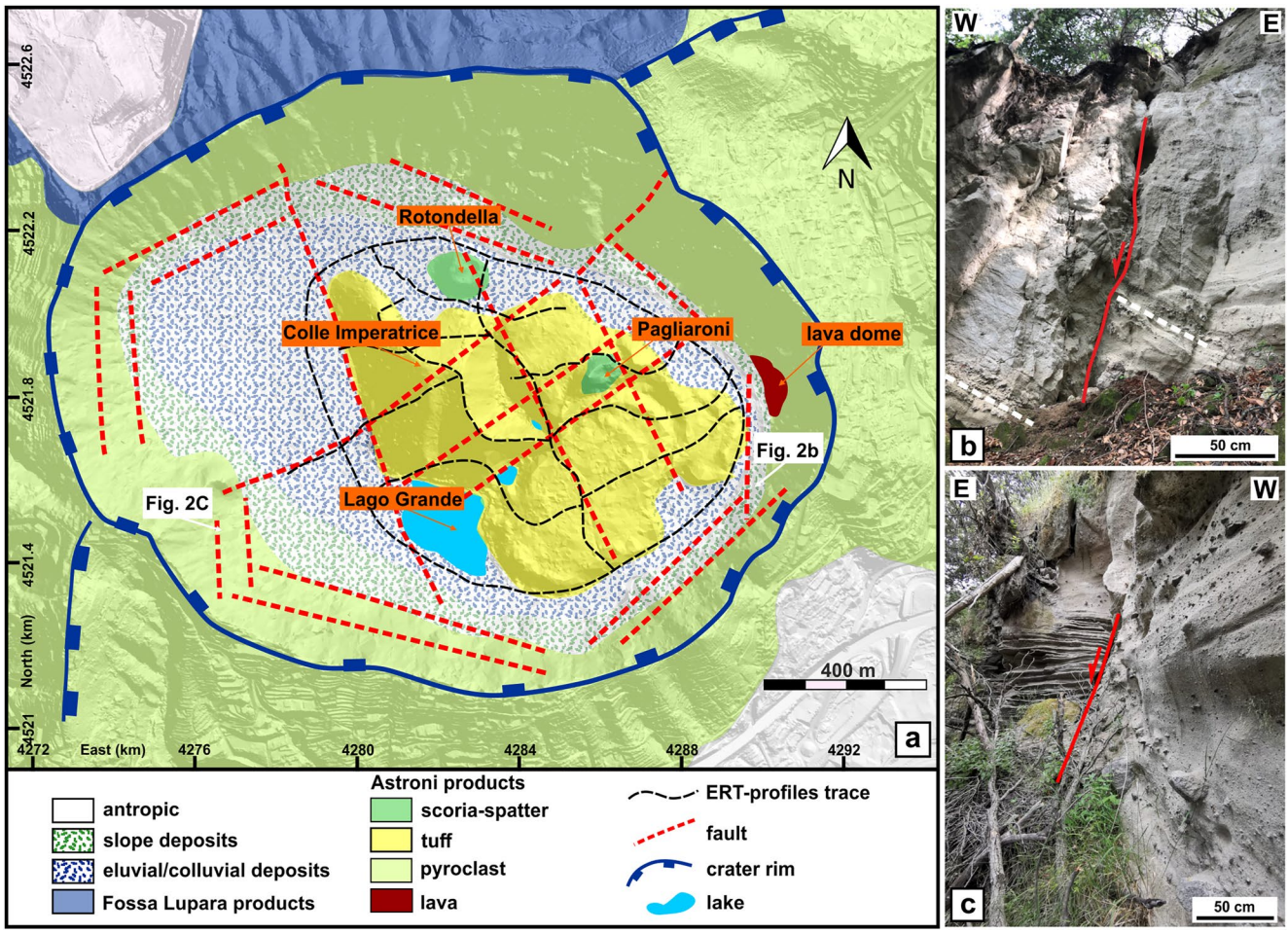

Figure 2. (a) Geological map of the Astroni Volcano also showing the profile traces of the geoelectrical survey. (b and c) Examples of ring faults.

1 hr and 6 days (Astbury et al., 2018) before the beginning of the Astroni 6 eruption, that is, the event with the highest magnitude in the entire eruptive sequence (Isaia et al., 2004).

The total duration of the seven eruptions was very short, ranging from years to decades (Isaia et al., 2004; Smith et al., 2011), and the eruptive vents were confined within the present Astroni crater (Figure 2a). The energy of the eruptive events was variable, with the sixth eruption forming a subplinian eruption column and likely enlarging the vent area to its present shape. The eruptions, being mainly characterized by phreatomagmatic activity, produced pyroclastic density currents (PDCs) mostly confined within the Campi Flegrei caldera margin (Isaia et al., 2004; Mele et al., 2015) and widespread pyroclastic deposits in a large area of the city of Naples and the Campanian Plain (Figure 1a). A lava dome was emplaced at the end of the Astroni 5 eruption (Figure 2a) and was later partly destroyed by the subplinian Astroni 6 eruption. The distribution and thickness of deposits, ballistic block trajectory, and facies architecture of the PDC (Isaia et al., 2004; Mele et al., 2015) suggest a possible temporal migration of the vents from the NW to the SE sector of the crater, which is also the most depressed area. The last volcanic activity was less energetic, forming small tuff cones (e.g., Colle dell'Imperatrice), spatter cones (e.g., Rotondella), and scoriae cones (e.g., Pagliaroni) within the crater floor, which also hosts three small lakes, the largest named Lago Grande (Figure 2a). New structural surveys have indicated that the eruptive activity resulted in a collapse of the crater floor through ring faults that were well exposed along the inner flanks of the Astroni tuff ring (Figures 2b and 2c). The data indicated that these structures include different faults oriented parallel to the volcano's inner flanks, exhibiting a broad tangential pattern with respect to the crater center. These areas were also the locations of several landslides.

A few hundred meters north of the Astroni Volcano edifice, three nested ring-shaped volcanic cones (i.e., Fossa Lupara; Figure 1a) formed following the Astroni emplacement. We note that the centers of these edifices are located along a NW–SE directed alignment passing through the Astroni vents (Figure 1a), which likely corresponds to a major eruptive fissure (Isaia et al., 2009). The Astroni eruptive events occurred at Campi Flegrei in the last epoch of activity between 5.5 and 3.8 ka (Smith et al., 2011) and are classified as small-to-medium-sized eruptions; the Astroni unit 6 has been used by the Italian Civil Protection as a representative eruptive scenario for hazard zonation in case of a renewal of volcanism.

3. Electrical Resistivity Survey

The geoelectrical technique reconstructs the electrical model of the subsoil using a controlled current injected into the ground through a couple of electrodes (i.e., source dipole) and the induced voltage drop in correspondence with other electrodes (i.e., receiving dipoles) (Loke & Barker, 1996). The source and receiving dipoles are displaced on the Earth's surface, following the topography. The measured potential difference is a function of the injected current, dipole geometry, and medium response (i.e., its apparent resistivity). Such measurements can be inverted to obtain electrical resistivity tomography (ERT) of the subsoil.

In recent decades, resistivity methods have been successfully applied in many different contexts, such as groundwater resources (e.g., Hermans et al., 2015; Yeh et al., 2015), fault imaging (e.g., Nguyen et al., 2005; Rizzo & Giampaolo, 2018; Suski et al., 2010; Troiano et al., 2009), the characterization of volcanoes and geothermal regions (e.g., Brothelande et al., 2014; Di Giuseppe, Troiano, & Carlino, 2017; Niccolin et al., 2006; Rosas-Carbajal et al., 2016; Tarchini et al., 2019; Troiano et al., 2008), the reconstruction of landslide structures (e.g., Lapenna et al., 2005; Lebourg et al., 2005), and geotechnical applications (e.g., Chambers et al., 2013; Sauret et al., 2015). The wide range of applications of these methods is a result of the large number of parameters influencing the electrical resistivity (e.g., porosity, fractures, rock/soil type, saturation, temperature, and fluid electrical conductivity) (Van Hoorde et al., 2017).

In this study, resistivity data were collected along 17 profiles (Figure 2a), with lengths between 480 and 840 m, adopting a dipole–dipole (DD) electrode configuration with 20 m spacing. In confined areas where it was difficult to manage cable layouts, as in the Astroni area, we found it effective to use the DD source–receiver coupling because it is more compact and sensitive to the lateral location and facilitates depth evaluation of anomaly source bodies (Ward, 1990). We used an Iris Syscal Pro instrument as a multichannel resistivitimeter, and employed it also as a power source, since it was able to produce direct current, with the maximum possible voltage and current being 800 V and 2 A, respectively.

Geological structures are three-dimensional; hence, to obtain accurate subsurface models, 3D acquisition and inversion techniques must be considered using arrays of electrodes laid on planes rather than on single lines (Loke et al., 2013). Indeed, complex heterogeneities cannot be adequately characterized using only 2D electrical resistivity surveys (Bentley & Gharibi, 2004). However, conducting full 3D surveys over large areas is difficult and time-intensive. Such setups are often not suitable because of their finite number of available acquisition channels, that is, cables and electrodes (Van Hoorde et al., 2017). To overcome the logistical constraints, 3D data sets can be collected from independent surveys along approximately straight lines displaced in mutually orthogonal directions, thereby acquiring data in more than one direction (e.g., Bentley & Gharibi, 2004; Berge & Drahor, 2011; Negri et al., 2008).

The ERT profile setup shown in Figure 2a was designed according to this rationale. The coverage appears dense, albeit irregular, with ERT profiles crossing the main geological structures, as already applied in other studies (Bouligand et al., 2019; Di Giuseppe et al., 2015; Revil et al., 2010). Consequently, 3D inversion of the data was deemed adequate. We note that the design of our experiment was heavily conditioned by the inaccessibility of some sectors of the Astroni crater.

The entire data set, consisting of 17 profiles in total, allowed for 3D inversion using the ERTlab3D® commercial software, including topography. The inversion procedure was based on the smoothness-constrained least squares inversion technique (LaBrecque et al., 1995). We used Occam's inverse algorithm (LaBrecque et al., 1995; Morelli & LaBrecque, 1996) to reconstruct the electrical resistivity image from electric potential data. Occam's inversion finds the smoothest possible model, whose response best fits the measured data to an a priori chi-square statistic (Constable et al., 1987; de Groot-Hedlin & Constaple., 1990). In the inversion routine, the subsurface

was divided into rectangular regions of constant resistivity, and the model smoothness was enforced by minimizing the differences in the log resistivity of adjacent blocks. The conjugate-gradient method was employed to solve both forward and inverse matrix systems, and a data-error reweighting scheme was implemented to suppress the effects of data outliers (Morelli & LaBrecque, 1996). The optimization method adjusts the resistivity model by iteratively reducing the difference between the calculated and measured apparent resistivity values; the root-mean-square (RMS) error provides a measure of this difference. The obtained RMS value was ∼5, which is compatible with the volcanic environment (Di Giuseppe et al., 2015; Di Giuseppe, Troiano, Di Vito, et al., 2017; Vargemezis, 2014).

As already discussed, a 3D model originating only from a series of in-line electrical resistivity measurements—like in our case—is not completely adequate for characterizing geometrically complex heterogeneities. Such a procedure might produce misleading models as a result of out-of-plane resistivity anomalies lying outside the survey lines. A series of techniques described by Loke and Dahlin (2010) have been adopted to avoid such possible artifacts in the final 3D inversion model, which often appear as banded near-surface anomalies aligned parallel (or perpendicular) to the surveillance lines. We adopted a higher damping factor for the model cells in the near-surface layers to reduce banding effects. In addition, we adopted a model discretization, such that the width and length of the model cells are similar, although the spacing between the lines is larger than the in-line electrode spacing. Finally, we modified the horizontal roughness filter to make it have components in the diagonal directions and in the directions along and perpendicular to the survey lines.

The final 3D model was supported by sensitivity analysis. The Jacobian (or sensitivity) matrix $S_{i,j}(\mathrm{m}) = \frac{\partial f_i(m)}{\partial m}$, containing the partial derivatives of the model responses with respect to the model parameters, was estimated using the ERTLab3D software, which provides a global sensitivity function equal to the diagonal of the matrix product $S^{\mathrm{T}}S$ and represents the sum (i.e., quadratic) of the sensitivities of all the quadrupoles (Sapia et al., 2021; Troiano et al., 2021). Considering that the absolute values of the sensitivity function may vary over a wide range, we computed a normalized sensitivity function, setting the maximum value to 100 and considering the 3% of the normalized sensitivity function as a good indication of the maximum resolution depth of our resistivity model. The unresolved areas are shown in Figure 3.

Our geophysical investigations focused on detecting the main rock formations, discontinuities, and fluid patterns down to about 150 m depth in an approximately 1,500 × 1,500 m^2 area covering the entire Astroni crater floor. Figure 3 shows three slices extracted by the 3D electrical model at different depths, that is, $z = 16$, -24, and -64 m above sea level (a.s.l.) (Figures 3a–3c).

The resistivity patterns of the horizontal tomograms presented diffuse heterogeneities with electrical resistivities ranging between a few and several hundred Ω·m (Figures 3a–3c); this was because expressions of the complex geology of the area were characterized by different lithological structures affected by faulting, fracturing, and alteration processes. Based on these three slices, the Astroni crater appeared to be separated into two sectors, both exhibiting a widely resistive electrical footprint (more than 100 Ω·m). Furthermore, the two sectors presented two conjugate trends in the NW–SE direction. The northernmost resistive anomaly had a NW–SE orientation, reaching a depth of approximately 70 m below sea level (b.s.l.), while the southernmost resistive anomaly had NE–SW orientation. The central sector of the crater was instead characterized by a conductive response (i.e., less than 100 Ω·m), detected in correspondence with the separation between the two resistive sectors described previously.

Six vertical resistivity cross-sections are depicted in Figure 3e; they were extracted by a 3D electrical model along the traces reported in Figure 3d to provide a clear view of the geometry of the detected anomalies, which reflect the volcanic and structural features identified in the area. Each of these sections was displaced close to and/or along with one of the measured profiles.

4. Gas Composition and Ground Temperature

To characterize the gas bubbles located in the E and NE sectors of Lago Grande, gas samples were collected using an upside-down plastic funnel positioned on a gas discharge. The funnel is connected through silicone tubes to a sampling glass flask with approximately 50 mL volume and equipped with two stopcocks. Gas samples were analyzed for both chemical (i.e., CO_2, Ar, N_2, O_2, CH_4, and He) and isotopic (i.e., $\delta^{13}C_{CO2}$ and $\delta^{18}O_{CO2}$) compositions at the INGV-OV laboratory of fluid geochemistry following Caliro et al. (2008). The analytical compositions are listed in Table 1.

10.1029/2022GC010534

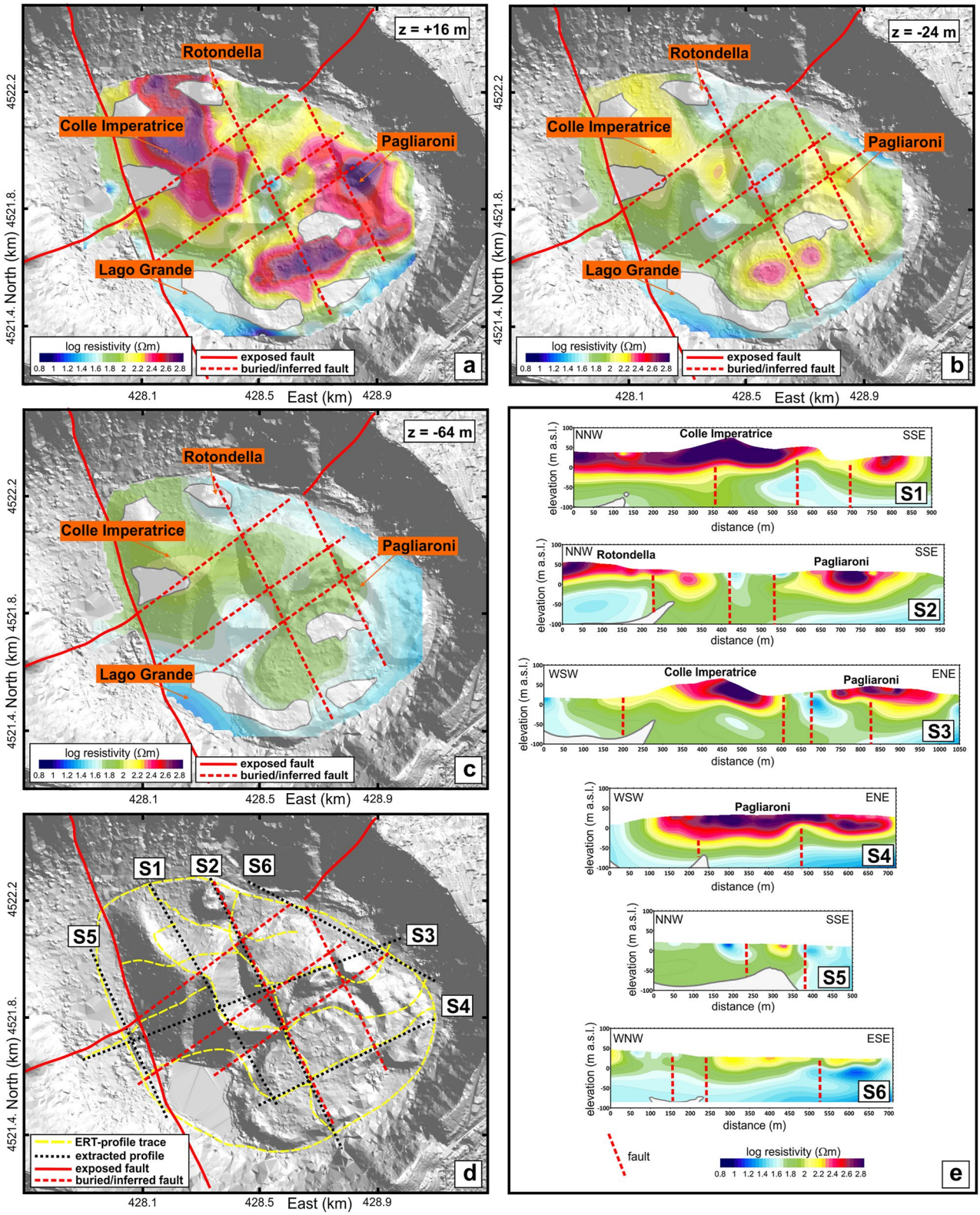

Figure 3. (a–c) Electrical resistivity maps at different depths. (d) Map of the Astroni crater showing the extracted profile traces of the electrical resistivity tomography and the mapped and inferred faults. (e) Electrical resistivity sections extracted by 3D modeling along traces shown in (d).

Table 1
Chemical and Isotopic Composition of Bubbling Gases Collected in the Eastern Sector of the Lago Grande

Sample	Date	Ar	O_2	N_2	CH_4	CO_2	He	$\delta^{13}C_{CO2}$	$\delta^{18}O_{CO2}$
Astroni_Lake1	19 July 2019	0.0422	0.38	1.92	0.11	97.91	0.000623	−1.84	33.80
Astroni_Lake2	19 May 2021	0.0269	0.02	1.26	0.114	98.58	0.000167	−2.27	32.47

Note. Concentrations are expressed in percent; isotopic compositions are in delta notation permill versus Vienna Pee Dee Belemnite.

We sampled the gas-bubbling manifestation in the NE sector of Lago Grande twice, where the bathymetry ranges between a few tens of centimeters and a couple of meters. Results indicated a CO_2-rich (i.e., ~98%) gas composition with minor amounts of atmospheric components and methane (i.e., ~0.1%). In the ternary diagram of Figure 4a, which shows the relative concentrations of the non-reactive gas species (i.e., He, N_2, and Ar), the gas-sample values range between the air-saturated water composition (ASW) and He and N_2 enriched component, suggesting the contribution of hydrothermal fluids, likely represented by the composition of Campi Flegrei fumaroles (Caliro et al., 2014); this is also supported by their isotopic composition (Table 1).

The ground temperature was also mapped in the area using a K-thermocouple for measuring the temperature at 30 cm depth. A total of 400 irregularly spaced data points (i.e., black points in Figures 4b and 4c) were used to produce a temperature map revealing the area with anomalous values. Ground-temperature data were processed using the commercial software Surfer, produced by Golden Software, using the point kriging geostatistical method to produce an interpolated grid (Isaaks & Srivastava, 1989). Temperature measurements were generally repeated every three to 4 months in the gas-emission area, starting from October 2019.

In the period from 2019 to the first trimester of 2022, the soil-temperature measurements (Figures 4b and 4c) revealed background values ranging from 10 to 24°C, while a 40°C maximum was measured in a narrow sector on the NE side of the lake (i.e., Lago Grande; Figures 3e and 4c), where an NNW–SSE trending anomaly (i.e., +24–40°C) was detected. The temperature values corresponding to the bubbling gas manifestation were quite constant during this period, with a difference of approximately 2°C between the measurements performed at 80 and 30 cm depth and within the 35–40°C range. The maximum measured temperatures were plotted in Figure 4d. This anomaly can be considered as a proxy for a structure that acts as a preferential pathway for rising fluids. However, the last measure of the temperature performed in September 2022 shows a maximum value of about 43°C at 30 cm depth, indicating a possible increase in fluid temperature rising from depth. However, this change in temperature anomaly needs to be verified as values and spatial distribution through new measurements in the following months.

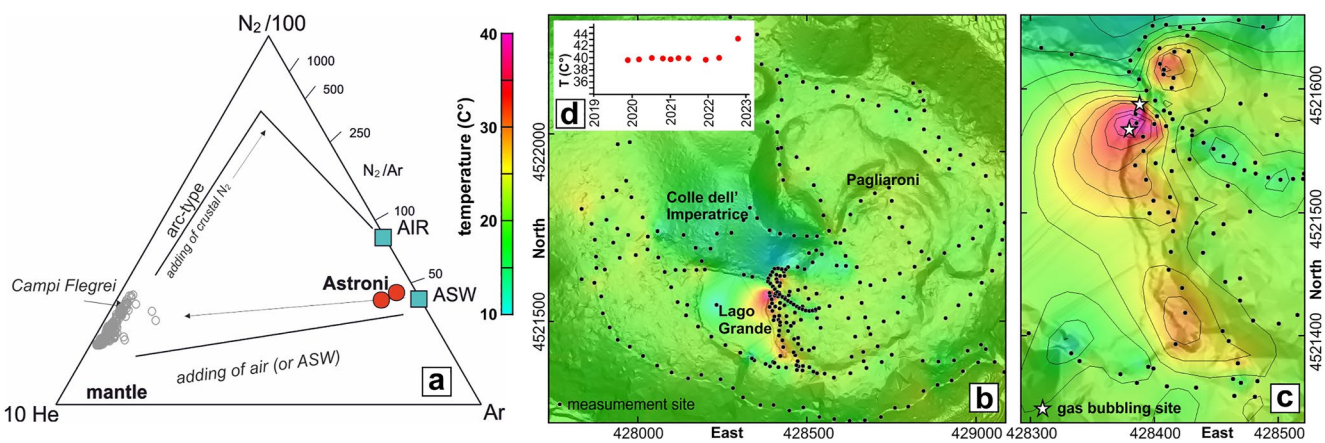

Figure 4. (a) Ternary plot showing the relative concentrations of the non-reactive gas species (i.e., He, N_2, and Ar). (b) Soil-temperature map. Black dots indicate the measurement locations. (c) Zoom of the Lago Grande NE side where the highest temperatures and gas bubbling occur. (d) Plot of the maximum measured temperatures.

5. Discussion

Combining new detailed volcano-tectonic analyses of the entire volcano and the previous volcanological reconstructions, we proposed an evolutionary model of the Astroni volcanic activity (Figure 5).

The Astroni Volcano formed along the border of the Agnano caldera following the Plinian Agnano-Monte Spina eruption (4.55 ka; de Vita et al., 1999; Smith et al., 2011). The eruptive activity produced at least seven small-to-medium magnitude eruptive events (Astroni 1–7) that happened over a total periods of years to few decades and were likely fed by a fissural system responsible for the variable vent opening during the eruptive activity (Figures 5a–5c). The prevailing explosive hydromagmatic activity was followed with the emplacement

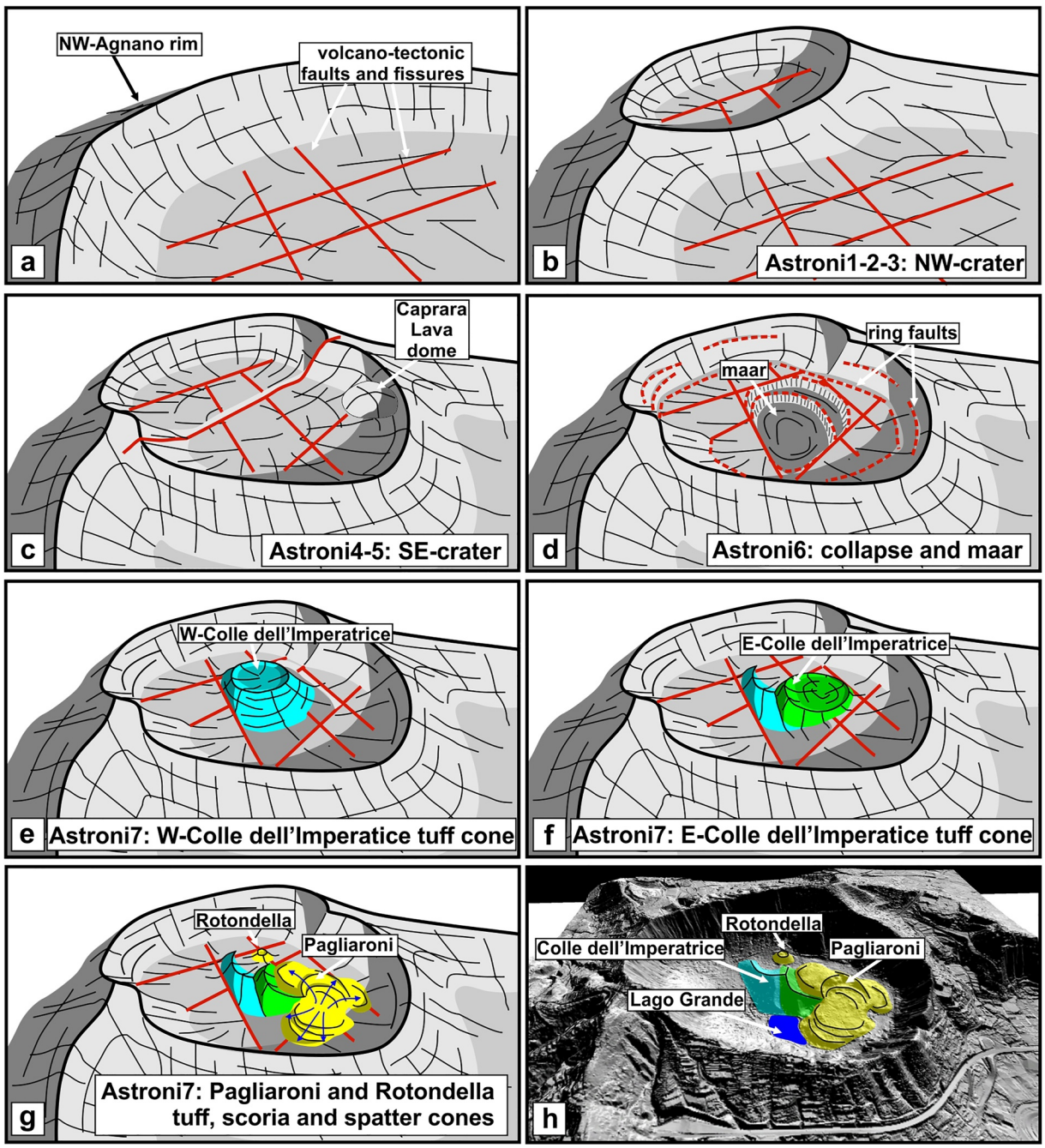

Figure 5. (a–h) Schematic evolutionary model of the volcano-tectonic events forming the present shape of the Astroni Volcano.

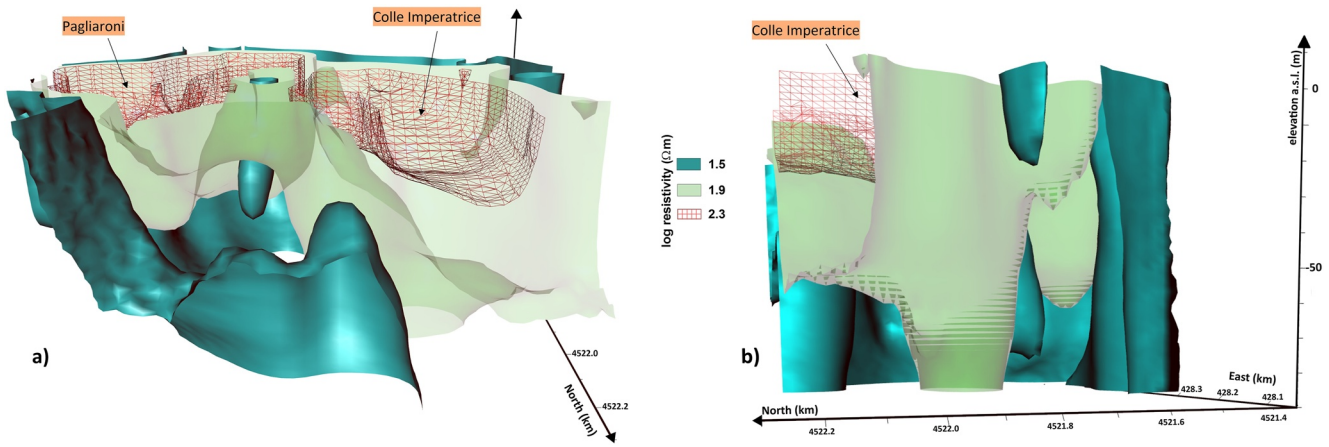

Figure 6. Sketches of the 3D resistivity model: blue, green and red correspond to the isosurfaces for ρ ~30, ~80, and ~200 Ω·m, respectively. (a) View S shows the Colle dell'Imperatrice and Pagliaroni structures highlighted by high values of resistivity (red isosurface). (b) View SE shows the root of Colle dell'Imperatrice cone marked by the 80 Ω·m isosurface (green).

of a lava dome along the eastern crater wall (Caprara Lava Dome), which closed the eruption event of Astroni 5. Volcanism resumption generated the larger subplinian eruption of Astroni 6 (Costa et al., 2009; Isaia et al., 2004; Mele et al., 2015), which produced a maar-like structure (Figure 5d) and mostly defined the present shape of the volcanic edifice. This structure was later partly covered by the pyroclastic deposits of the subsequent Astroni 7 eruptive event, which also generated the volcanic structures associated to the final activity of Astroni volcano (Figures 5e–5g). The Astroni 7 eruptive event include the production of tuff, spatter, scoriae, and highly crystalline frothy rock bodies preserved on the crater floor (Figure 5h) and were further investigated and defined by ERT.

In this study, we presented a 3D ERT of the shallower part of the Astroni crater, with the aim of defining down to 150 m depth the geometry of the main structures exposed in the crater. The extracted vertical resistivity cross-sections indicate that a resistive body occurs in correspondence with the Colle Imperatrice volcanic structure down to the investigation depth (i.e., S1 and S3 sections in Figure 3e). A shallower resistive structure with an articulated shape is imaged close to the Pagliaroni structure (i.e., S2, S3, and S4 sections in Figure 3e); the latter includes a flatter resistivity anomaly around the NE–SW extension (i.e., S4 section in Figure 3e), which perfectly encompasses the morphology highlighted by the digital terrain model (DTM) of the crater. A third known volcanic structure, that is, the Rotondella spatter cone, has not been precisely captured by the final 3D resistivity model, consequently of its sensitivity limits in this sector. A resistive anomaly at the NNW corner of the S2 section can be the signal of the rocks of the Rotondella small vent (Figure 3e).

The geometry of the anomalies confirms the stratigraphic reconstruction and indicates that Pagliaroni is the most recent vent. The peripheral resistivity cross-sections, namely S5 and S6 (Figure 3e), reveal a prevailing conductive volume encompassing the lateral extension of the previously described structures. Resistivity contrasts indicate the presence of discontinuities in the subsurface corresponding to faults and/or fracturing zones; however, some of the faults seem to be covered by resistive bodies corresponding to the deposits of Pagliaroni and Colle Imperatrice (e.g., S3 and S4 sections in Figure 3e), suggesting that they are related to previous volcano-tectonic events likely due to the maar-like structure during Astroni 6 eruptive event. The electrical tomograms reveal how resistive bodies characterize the northwestern and southeastern sectors of the crater; such sectors appear separated by a conductive structure with NE–SW orientation, corresponding to the central part of the crater (Figure 3).

The geometry of the resistive bodies perfectly matches the morphology of the surficial volcanic structures identified in the field, such as Colle Imperatrice and Pagliaroni cones. It is also highlighted by structural analyses of the high-resolution DTM of the densely vegetated crater area. The imaged electrical anomalies linked to the stratigraphic relationships, geometry, and position of these structures suggest a migration of the activity likely along the faults bordering the maar-like crater, likely located in the center, that formed after the Astroni 6 subplinian eruption, which might also represent a shallow sector of an eruptive fissure.

The 3D ERT reconstructed the deep roots of the Colle dell'Imperatrice cone, as shown in Figure 6, where the selected resistivity isosurfaces depict a vertical conduit developed at depth (ρ = ~80 Ω•m), as well as the shallower resistive structures of other small volcanic edifices (ρ = ~200 Ω·m). The 3D resistivity model shows the shape of the Pagliaroni edifice, which includes a shallow resistive body with a tabular shape (S4 section in Figure 3e). These volcanic edifices are mainly NW–SE aligned and bounded in the south-southeastern sector by the area mainly occupied by Lago Grande.

The conductive structure (ρ = ~30 Ω·m) situated in the central sector of the Astroni crater also presents deep roots for the source area of Colle dell'Imperatrice tuff cone, at least down to the maximum investigated depth (approximately 150 m) in the present ERT survey (Figures 3 and 5). This feature, which cuts the Astroni crater into two sectors, represents the link with the conduit at depth, possibly related to a maar-like structure. The southernmost high-resistivity tabular volcanic structure, which is composed of frothy lavas enriched in crystals, could be the result of the final spreading of a very degassed and viscous magma along with a shallow sector of the eruptive fissure or following a lateral partial collapse of the Pagliaroni cone (Figure 6) which produced a lava coulée, similar to other volcanic systems (De Silva et al., 1994). The major faults reconstructed by the anomalies detected by the 3D resistivity model (Figures 3a–3c) indicate that there are two main sets characterized by the NE–SW and NW–SE regional directions, which generally prevail throughout the Campi Flegrei caldera (Vitale & Isaia, 2014; Natale, Camanni, et al., 2022; Natale, Ferranti, et al., 2022). Furthermore, the NW–SE direction is the same as the already hypothesized larger-scale eruptive fissure (Isaia et al., 2009). This main volcano-tectonic structure is part of the alignment of positive gravity and magnetic anomalies (i.e., Mt. Spina, Astroni, and Fossa Lupara volcanoes in Figure 1a) evident in the high-pass filter maps of the Bouguer anomaly and pole-reduced magnetic field in Barberi et al. (1991).

The detected resistivity anomalies combined with the identified structural features suggest the presence of active structures within the Astroni Volcano that convey the upward migration of hydrothermal fluids. It is worth noting that the bubbling manifestation within Lago Grande is localized along the border of the Pagliaroni lava coulée and likely along the ring faults bounding the maar structure (Figure 7). Furthermore, the gas composition (Figure 4a) suggests a possible contribution from hydrothermal fluids, such as those discharged by the Solfatara fumaroles (Caliro et al., 2014). The CO_2 carbon isotopic composition of −1.84/−2.27‰ $\delta^{13}C$ (vs. V-PDB; Vienna Pee Dee Belemnite) is comparable to the composition of the fluids released by the Solfatara fumaroles (i.e., −1.4 ± 0.4‰; Caliro et al., 2014), thereby suggesting the same hydrothermal origin of the fluids discharged in the Astroni crater lake. The fluid-emission area is also marked by a soil-temperature anomaly (Figures 4b–4d) that extends along the northeastern margin of the lake, with a maximum value of 40/43°C. This area also corresponds to the border between the southernmost and youngest volcanic structures identified within the crater (Figure 7). Historical chronicles (i.e., Barbati, 1995) report a thermal bath (i.e., *Balneum Astruni*) within the Astroni Volcano, which King Federico II used in 1217 CE for curative therapies, while the exploitation of thermo-mineral springs in Campi Flegrei declined after the volcanic phenomena accompanying the eruption of Monte Nuovo in 1538 CE (Giacomelli & Scandone, 2012). Young et al. (2020) discovered a gravity anomaly (Figure 8) beneath the Astroni Volcano, formed by a fluid-dominated and highly fractured geothermal reservoir; they hypothesize that the reservoir is trapped beneath a less permeable cap rock at the time of the survey. The authors also suggested that seismicity in the area may be due to the movement of fluids mainly along the NW–SE and NE–SW to NNE–SSW oriented faults, which can act as fluid pathways linking the Solfatara/Pisciarelli and Astroni volcanoes (Figure 8). The reservoir is likely confined within the SW sector of the Astroni crater by a NW–SE oriented structure highlighted by our ERT imaging and corresponds to the limit of the resistivity anomaly of the Colle dell'Imperatrice tuff cone (Figures 3 and 7). Investigations using SAR and seismic interferometric methods of volcanic structures at Campi Flegrei (Pepe et al., 2019) also highlighted that the spatial distribution of seismicity coincides with the extinct volcanic vents/plumbing system in the eastern part of the caldera (i.e., Solfatara/Pisciarelli and Astroni volcanoes), thereby constraining or channeling the eastward propagation of magmatic and hydrothermal fluids. In addition, in this sector of the caldera, we also recorded a significant variation in hydrothermal activity, which was verified by an increased degassing process (Cardellini et al., 2017) and warming of the hydrothermal system (Chiodini et al., 2015), and may imply a larger area involved during periods of unrest (e.g., Sabbarese et al., 2020).

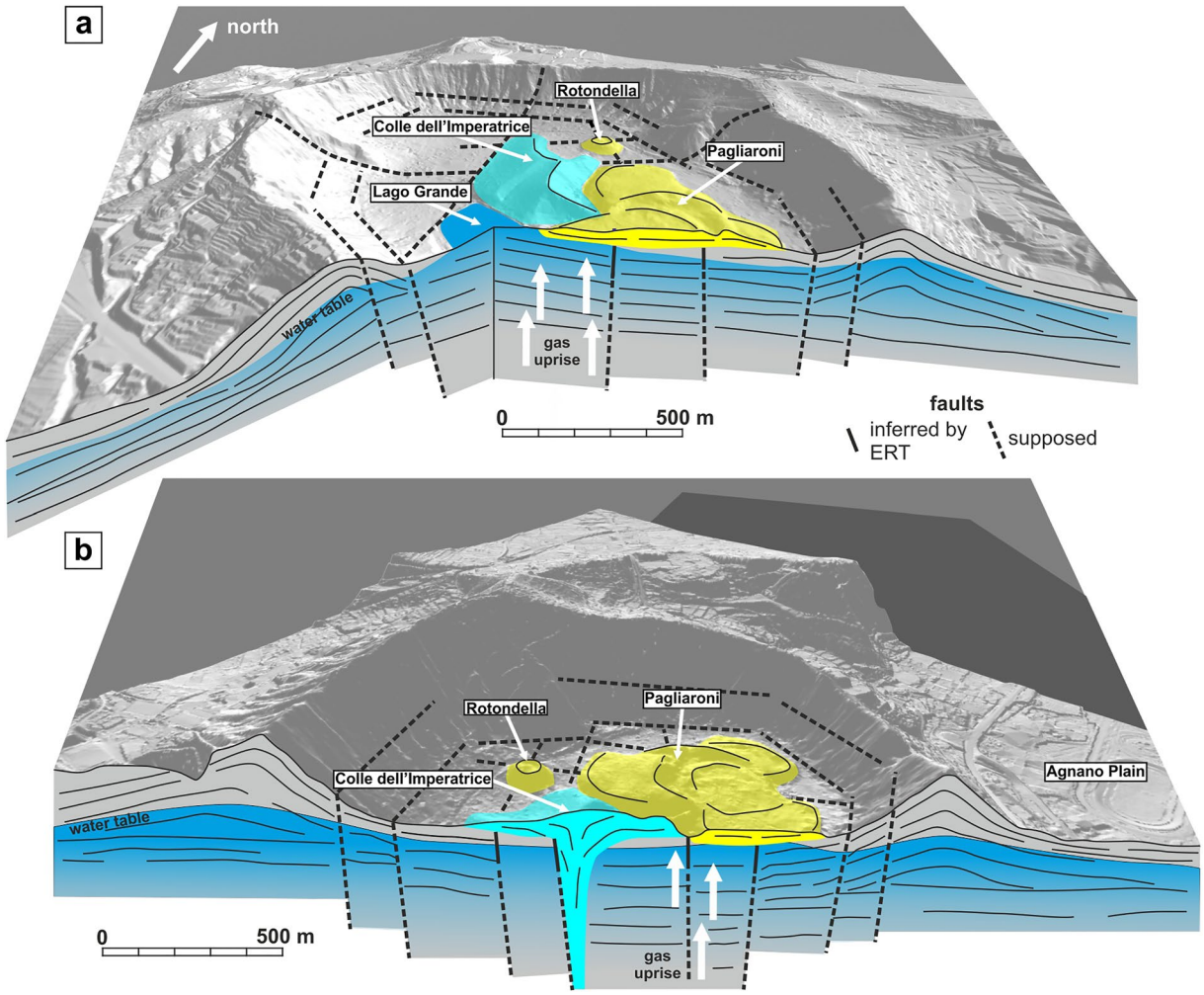

Figure 7. The 3D scheme of the volcano-tectonic structure of the Astroni Volcano, revealing the main features and ongoing degassing beneath Lago Grande. (a) View NNE shows the gas rising below the NE side of the Lago Grande and the western sector of Pagliaroni lava culeé. (b) View NW shows the Colle dell'Imperatrice root and gas rising below the Pagliaroni lava culeé.

6. Conclusive Remarks

The presented multidisciplinary study provided a more detailed volcano-tectonic architecture of this volcano, allowing us to reconstruct its evolution and current activity. We elucidated the deep geometry of the main structures linked to the vents that operate during the final stages of eruptive activity and the major structural discontinuities through which the observed and analyzed hydrothermal liquids, and gases rise to the surface. The geophysical and geochemical anomalies detected within the Astroni Volcano suggested a possible involvement of this area in the seismic and hydrothermal activity that recently occurred in the central sector of the Campi Flegrei caldera. The chemical affinities of the analyzed gases and those emitted in the Solfatara-Pisciarelli area also suggest that further surveys should identify the possible deep structure that connects the Astroni Volcano with the neighboring most active area of the caldera, as already suggested in previous studies and will also help to evaluate better the dynamics and evolution of the Astroni Volcano, which in recent years was also a site of seismic activity both as swarms or shocks. Additional investigations of the whole volcanic structure to detect other possible geophysical and geochemical anomalies besides those presented in this study will also allow for planning regular monitoring of the anomalies recorded and better evaluate the evolution of the unrest crisis at the Campi Flegrei, for which the alert level was raised to yellow by the Italian Civil Protection since 2012.

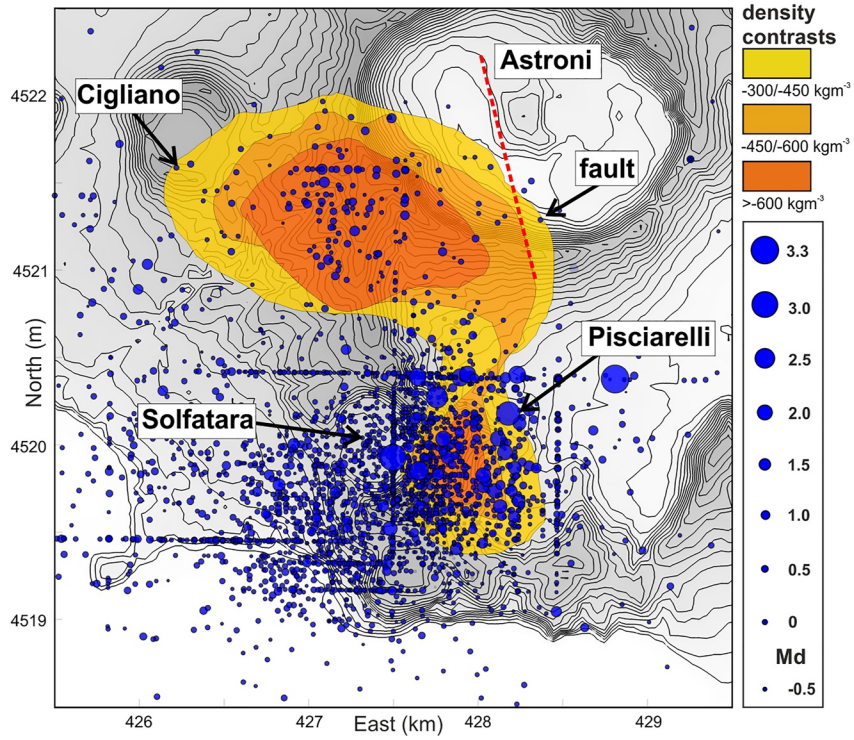

Figure 8. Sketch map showing the surface traces of anomalous bodies for density contrasts of −600, −450, and −300 kg·m^{-3} (Young et al., 2020), and the earthquake hypocenters in 2000–2021 at the central sector of Campi Flegrei (The E–W and N–S hypocenter alignments are artifacts related to the low spatial resolution of the low-magnitude earthquakes).

Conflict of Interest

The authors declare no conflicts of interest relevant to this study.

Data Availability Statement

The electrical resistivity and temperature data sets used in this work are available in the following repository: Isaia et al. (2022).

Acknowledgments

We are grateful to the Editor Claudio Faccenna, the reviewer Michael Ort, and an anonymous referee for the useful and constructive suggestions that improved this paper. We warmly thank F.D.A Tramparulo for the help during the Geoelectric and Ground Temperature surveys. We thank J. Natale for the elaboration of the DTM of the Astroni area; L. Cascini, J. Natale, and D. Sparice for their help in the field activities; and director F. Canonico and the staff of the Oasi WWF Cratere degli Astroni (https://crateredegliastroni.org) for allowing us to perform the survey and providing logistic support. This work was partly funded by the INGV Ricerca Libera 2019 project "Structural setting and volcano-tectonic evolution of the Astroni Volcano: implication on its present state and dynamics."

References

Acocella, V. (2007). Understanding caldera structure and development: An overview of analogue models compared to natural calderas. *Earth-Science Reviews*, *85*(3–4), 125–160. https://doi.org/10.1016/j.earscirev.2007.08.004

Acocella, V., Di Lorenzo, R., Newhall, C., & Scandone, R. (2015). An overview of recent (1988 to 2014) caldera unrest: Knowledge and perspectives. *Reviews of Geophysics*, *53*(3), 896–955. https://doi.org/10.1002/2015RG000492

Astbury, R. L., Petrelli, M., Ubide, T., Stock, M. J., Arienzo, I., D'Antonio, M., & Perugini, D. (2018). Tracking plumbing system dynamics at the Campi Flegrei caldera, Italy: High-resolution trace element mapping of the Astroni crystal cargo. *Lithos*, *318–319*, 464–477. https://doi.org/10.1016/j.lithos.2018.08.033

Barbati, S. (1995). *L'antico itinerario delle terre flegree: Ricostruzioni dalle immagini in Le terme puteolane e Salerno nei codici miniati di Pietro da Eboli* (pp. 57–109). Fausto Fiorentino. (Bartolo 1995).

Barberi, F., Cassano, E., La Torre, P., & Sbrana, A. (1991). Structural evolution of Campi Flegrei caldera in light of volcanological and geophysical data. *Journal of Volcanology and Geothermal Research*, *48*(1–2), 33–49. https://doi.org/10.1016/0377-0273(91)90031-T

Battaglia, J., Zollo, A., Virieux, J., & Dello Iacono, D. (2008). Merging active and passive data sets in traveltime tomography: The case study of Campi Flegrei caldera (Southern Italy). *Geophysical Prospecting*, *56*(4), 555–573. https://doi.org/10.1111/j.1365-2478.2007.00687

Bentley, L. R., & Gharibi, M. (2004). Two- and three-dimensional electrical resistivity imaging at a heterogeneous remediation site. *Geophysics*, *69*(3), 674–680. https://doi.org/10.1190/1.1759453

Berge, M. A., & Drahor, M. G. (2011). Electrical resistivity tomography investigations of multilayered archaeological settlements: Part I–modelling. *Archaeological Prospection*, *18*(3), 159–171. https://doi.org/10.1002/arp.414

Bevilacqua, A., Flandoli, F., Neri, A., Isaia, R., & Vitale, S. (2016). Temporal models for the episodic volcanism of Campi Flegrei caldera (Italy) with uncertainty quantification. *Journal of Geophysical Research: Solid Earth*, *121*(11), 7821–7845. https://doi.org/10.1002/2016JB013171

Bevilacqua, A., Isaia, R., Neri, A., Vitale, S., Aspinal, W. P., Bisson, M., et al. (2015). Quantifying volcanic hazard at Campi Flegrei caldera (Italy) with uncertainty assessment: I. Vent opening maps. *Journal of Geophysical Research: Solid Earth*, *120*(4), 2309–2329. https://doi.org/10.1002/2014JB011775

Bouligand, C., Hurwitz, S., Vandemeulebrouck, J., Byrdina, S., Kass, M. A., & Lewicki, J. L. (2019). Heat and mass transport in a vapor-dominated hydrothermal area in Yellowstone National Park, USA: Inferences from magnetic, electrical, electromagnetic, subsurface temperature, and diffuse CO_2 flux measurements. *Journal of Geophysical Research: Solid Earth*, *124*(1), 291–309. https://doi.org/10.1029/2018JB016202

Brothelande, E., Finizola, A., Peltier, A., Delcher, E., Komorowski, J. C., Di Gangi, F., et al. (2014). Fluid circulation pattern inside La Soufrière volcano (Guadeloupe) inferred from combined electrical resistivity tomography, self-potential, soil temperature and diffuse degassing measurements. *Journal of Volcanology and Geothermal Research*, *288*, 105–122. https://doi.org/10.1016/j.jvolgeores.2014.10.007

Byrdina, S., Vandemeulebrouck, J., Cardellini, C., Legaz, A., Camerlynck, C., Chiodini, G., et al. (2014). Relations between electrical resistivity, carbon dioxide flux, and self-potential in the shallow hydrothermal system of Solfatara (Phlegrean Fields, Italy). *Journal of Volcanology and Geothermal Research*, *283*, 172–182. https://doi.org/10.1016/j.jvolgeores.2014.07.010

Caliro, S., Chiodini, G., Izzo, G., Minopoli, C., Signorini, A., Avino, R., & Granieri, D. (2008). Geochemical and biochemical evidence of lake overturn and fish kill at Lake Averno, Italy. *Journal of Volcanology and Geothermal Research*, *178*(2), 305–316. https://doi.org/10.1016/j.jvolgeores.2008.06.023

Caliro, S., Chiodini, G., & Paonita, A. (2014). Geochemical evidences of magma dynamics at Campi Flegrei (Italy). *Geochimica et Cosmochimica Acta*, *132*, 1–15. https://doi.org/10.1016/j.gca.2014.01.021

Calò, M., & Tramelli, A. (2018). Anatomy of the Campi Flegrei caldera using enhanced seismic tomography models. *Scientific Reports*, *8*(1), 16254. https://doi.org/10.1038/s41598-018-34456-x

Capuano, P., Russo, G., Civetta, L., Orsi, G., D'Antonio, M., & Moretti, R. (2013). The active portion of the Campi Flegrei caldera structure imaged by 3-D inversion of gravity data. *Geochemistry, Geophysics, Geosystems*, *14*(10), 4681–4697. https://doi.org/10.1002/ggge.20276

Cardellini, C., Chiodini, G., Frondini, F., Avino, R., Bagnato, E., Caliro, S., et al. (2017). Monitoring diffuse volcanic degassing during volcanic unrests: The case of Campi Flegrei (Italy). *Scientific Reports*, *7*(1), 6757. https://doi.org/10.1038/s41598-017-06941-2

Chambers, J. E., Wilkinson, P. B., Penn, S., Meldrum, P. I., Kuras, O., Loke, M. H., & Gunn, D. A. (2013). River terrace sand and gravel deposit reserve estimation using three-dimensional electrical resistivity tomography for bedrock surface detection. *Journal of Applied Geophysics*, *93*, 25–32. https://doi.org/10.1016/j.jappgeo.2013.03.002

Chiodini, G., Vandemeulebrouck, J., Caliro, S., D'Auria, L., De Martino, P., Mangiacapra, A., & Petrillo, Z. (2015). Evidence of thermal-driven processes triggering the 2005–2014 unrest at Campi Flegrei caldera. *Earth and Planetary Science Letters*, *414*, 58–67. https://doi.org/10.1016/j.epsl.2015.01.012

Constable, S. C., Parker, R. L., & Constable, C. G. (1987). Occam's inversion: A practical algorithm for generating smooth models from electromagnetic sounding data. *Geophysics*, *52*(3), 289–300. https://doi.org/10.1190/1.1442303

Costa, A., Dell'Erba, F., Di Vito, M. A., Isaia, R., Macedonio, G., Orsi, G., & Pfeiffer, T. (2009). Tephra fallout hazard assessment at the Campi Flegrei caldera (Italy). *Bulletin of Volcanology*, *71*(3), 259–273. https://doi.org/10.1007/s00445-008-0220-3

de Groot-Hedlin, C., & Constable, S. (1990). Occam's inversion to generate smooth, two-dimensional models from magnetotelluric data. *Geophysics*, *55*(12), 1613–1624. https://doi.org/10.1190/1.1442813

De Siena, L., Chiodini, G., Vilardo, G., Del Pezzo, E., Castellano, M., Colombelli, S., et al. (2017). Source and dynamics of a volcanic caldera unrest: Campi Flegrei, 1983–84. *Scientific Reports*, *7*(1), 8099. https://doi.org/10.1038/s41598-017-08192-7

De Siena, L., Del Pezzo, E., & Bianco, F. (2010). Seismic attenuation imaging of Campi Flegrei: Evidence of gas reservoirs, hydrothermal basins, and feeding systems. *Journal of Geophysical Research*, *115*(B9), B09312. https://doi.org/10.1029/2009JB006938

De Silva, S. L., Self, S., Francis, P. W., Drake, R. E., & Carlos, R. R. (1994). Effusive silicic volcanism in the Central Andes: The chao dacite and other young lavas of the Altiplano Puna Volcanic Complex. *Journal of Geophysical Research*, *99*(B9), 17805–17825. https://doi.org/10.1029/94JB00652

de Vita, S., Orsi, G., Civetta, L., Carandente, A., D'Antonio, M., Deino, A., et al. (1999). The Agnano–Monte Spina eruption (4.1 ka) in the resurgent, nested Campi Flegrei caldera (Italy). *Journal of Volcanology and Geothermal Research*, *91*(2–4), 269–301. https://doi.org/10.1016/S0377-0273(99)00039-6

Di Giuseppe, M. G., & Troiano, A. (2019). Monitoring active fumaroles through time-lapse electrical resistivity tomograms: An application to the Pisciarelli fumarolic field (Campi Flegrei, Italy). *Journal of Volcanology and Geothermal Research*, *375*, 32–42. https://doi.org/10.1016/j.jvolgeores.2019.03.009

Di Giuseppe, M. G., Troiano, A., & Carlino, S. (2017). Magnetotelluric imaging of the resurgent caldera on the island of Ischia (Southern Italy): Inferences for its structure and activity. *Bulletin of Volcanology*, *79*(12), 85. https://doi.org/10.1007/S00445-017-1170-4

Di Giuseppe, M. G., Troiano, A., Di Vito, M., Somma, R., & Matano, F. (2017). Definition of small-scale volcanic structures by electrical resistivity tomography: The Trentaremi cone, an example from the Campi Flegrei caldera (Italy). *Annals of Geophysics*, *60*(5), 0552. https://doi.org/10.4401/ag-7397

Di Giuseppe, M. G., Troiano, A., Fedele, A., Caputo, T., Patella, D., Troise, C., & De Natale, G. (2015). Electrical resistivity tomography imaging of the near-surface structure of the Solfatara Crater, Campi Flegrei (Naples, Italy). *Bulletin of Volcanology*, *77*(4), 27. https://doi.org/10.1007/s00445-015-0910-6

Di Vito, M. A., Isaia, R., Orsi, G., Southon, J., de Vita, S., D'Antonio, M., et al. (1999). Volcanism and deformation since 12, 000 years at the Campi Flegrei caldera Italy. *Journal of Volcanology and Geothermal Research*, *91*(2–4), 221–246. https://doi.org/10.1016/S0377-0273(99)00037-2

Geyer, A., & Martì, J. (2014). A short review of our current understanding of the development of ring faults during collapse caldera formation. *Frontiers of Earth Science*, *2*, 22. https://doi.org/10.3389/feart.2014.00022

Giacomelli, L., & Scandone, R. (2012). History of the exploitation of thermos mineral resources in Campi Flegrei and Ischia, Italy. *Journal of Volcanology and Geothermal Research*, *209–210*, 19–32. https://doi.org/10.1016/j.jvolgeores.2011.10.004

Gottsmann, J., Carniel, R., Coppo, N., Wooller, L., Hautmann, S., & Rymer, H. (2007). Oscillations in hydrothermal systems as a source of periodic unrest at caldera volcanoes: Multiparameter insights from Nisyros, Greece. *Geophysical Research Letters*, *34*(7), L07307. https://doi.org/10.1029/2007GL029594

Gresse, M., Vandemeulebrouck, J., Byrdina, S., Chiodini, G., Revil, A., Johnson, T. C., et al. (2017). Three-dimensional electrical resistivity tomography of the Solfatara crater (Italy): Implication for the multiphase flow structure of the shallow hydrothermal system. *Journal of Geophysical Research: Solid Earth*, *122*(11), 8749–8768. https://doi.org/10.1002/2017JB014389

Hermans, T., Nguyen, F., & Caers, J. (2015). Uncertainty in training image-based inversion of hydraulic head data constrained to ERT data: Workflow and case study. *Water Resources Research*, *51*(7), 5332–5352. https://doi.org/10.1002/2014WR016460

Isaaks, E. H., & Srivastava, M. R. (1989). *Applied Geostatistics*. Oxford University Press.

Isaia, R., D'Antonio, M., Dell' Erba, F., Di Vito, M., & Orsi, G. (2004). The Astroni volcano: The only example of close eruptions within the same vent area in the recent history of the Campi Flegrei caldera (Italy). *Journal of Volcanology and Geothermal Research*, *133*(1–4), 171–192. https://doi.org/10.1016/S0377-0273(03)00397-4

Isaia, R., Di Giuseppe, M. G., Natale, J., Tramparulo, F. D. A., Troiano, A., & Vitale, S. (2021). Volcano tectonic setting of the Pisciarelli Fumarole Field, Campi Flegrei caldera, Southern Italy: Insights into fluid circulation patterns and hazard scenarios. *Tectonics*, *40*(5), e2020TC006227. https://doi.org/10.1029/2020TC006227

Isaia, R., Di Giuseppe, M. G., Troiano, A., Avino, R., Caliro, S., Santi, A., & Vitale, S. (2022). Electrical resistivity and temperature datasets from "Structure and present state of the Astroni Volcano in the Campi Flegrei caldera (Italy) based on multidisciplinary investigations". figshare. [Dataset]. https://doi.org/10.6084/m9.figshare.21518559.v3

Isaia, R., Marianelli, P., & Sbrana, R. (2009). Caldera unrest prior to intense volcanism in Campi Flegrei (Italy) at 4.0 ka B.P.: Implications for caldera dynamics and future eruptive scenarios. *Geophysical Research Letters*, *36*(21), L21303. https://doi.org/10.1029/2009GL040513

Isaia, R., Vitale, S., Di Giuseppe, M. G., Iannuzzi, E., D'Assisi Tramparulo, F., & Troiano, A. (2015). Stratigraphy, structure, and volcano-tectonic evolution of Solfatara maar-diatreme (Campi Flegrei, Italy). *The Geological Society of America Bulletin*, *127*(9–10), 1485–1504. https://doi.org/10.1130/B31183.1

Kennedy, B. M., Holohan, E. P., Stix, J., Gravley, D. M., Davidson, L. R. J., & Cole, J. W. (2018). Magma plumbing beneath collapse caldera volcanic systems. *Earth-Science Reviews*, *177*, 404–424. https://doi.org/10.1016/j.earscirev.2017.12.002

LaBrecque, D. J., Morelli, G., Daily, B., Ramirez, A., & Lundegard, P. (1995). Occam's inversion of 3-D ERT data. In B. Spies (Ed.), *Three-dimensional electromagnetics* (pp. 575–590). SEG.

Lapenna, V., Lorenzo, P., Perrone, A., Piscitelli, S., Rizzo, E., & Sdao, F. (2005). 2D electrical resistivity imaging of some complex landslides in Lucanian Apennine chain, Southern Italy. *Geophysics*, *70*(3), B11–B18. https://doi.org/10.1190/1.1926571

Lebourg, T., Binet, S., Tric, E., Jomard, H., & El Bedoui, S. (2005). Geophysical survey to estimate the 3D sliding surface and the 4D evolution of the water pressure on part of a deep seated landslide. *Terra Nova*, *17*(5), 399–406. https://doi.org/10.1111/j.1365-3121.2005.00623.x

Loke, M. H., & Barker, R. D. (1996). Rapid least-squares inversion of apparent resistivity pseudosections by a quasi-Newton method. *Geophysical Prospecting*, *44*(1), 131–152. https://doi.org/10.1111/j.1365-2478.1996.tb00142.x

Loke, M. H., Chambers, J. E., Rucker, D. F., Kuras, O., & Wilkinson, P. B. (2013). Recent developments in the direct-current geoelectrical imaging method. *Journal of Applied Geophysics*, *95*, 135–156. https://doi.org/10.1016/j.jappgeo.2013.02.017

Loke, M. H., & Dahlin, T. (2010). Methods to reduce banding effects in 3-D resistivity inversion. In *Near Surface 2010-16th EAGE European Meeting of Environmental and Engineering Geophysics*. European Association of Geoscientists & Engineers.cp-164.

Martí, J., Geyer, A., Folch, A., & Gottsmann, J. (2008). A review on collapse caldera modelling. *Developments in Volcanology*, *10*, 233–283. https://doi.org/10.1016/S1871-644X(07)00006-X

Mele, D., Dioguardi, F., Dellino, P., Isaia, R., Sulpizio, R., & Braia, G. (2015). Hazard of pyroclastic density currents at the Campi Flegrei caldera (Southern Italy) as deduced from the combined use of facies architecture, physical modeling and statistics of the impact parameters. *Journal of Volcanology and Geothermal Research*, *299*, 35–53. https://doi.org/10.1016/j.jvolgeores.2015.04.002

Morelli, G., & LaBrecque, D. J. (1996). Advances in ERT inverse modelling. *European Journal of Environmental and Engineering Geophysics*, *1*(2), 171–186.

Natale, J., Camanni, G., Ferranti, L., Isaia, R., Sacchi, M., Spiess, V., et al. (2022). Fault systems in the offshore sector of the Campi Flegrei caldera (Southern Italy): Implications for nested caldera structure, resurgent dome, and volcano-tectonic evolution. *Journal of Structural Geology*, *163*, 104723. https://doi.org/10.1016/j.jsg.2022.104723

Natale, J., Ferranti, L., Isaia, R., Marino, C., Sacchi, M., Spiess, V., et al. (2022). Integrated on-land-offshore stratigraphy of the Campi Flegrei caldera: New insights into the volcano-tectonic evolution in the last 15 kyr. *Basin Research*, *34*(2), 855–882. https://doi.org/10.1111/bre.12643

Negri, S., Leucci, G., & Mazzone, F. (2008). High resolution 3D ERT to help GPR data interpretation for researching archaeological items in a geologically complex subsurface. *Journal of Applied Geophysics*, *65*(3–4), 111–120. https://doi.org/10.1016/j.jappgeo.2008.06.004

Nguyen, F., Garambois, S., Jongmans, D., Pirard, E., & Loke, M. H. (2005). Image processing of 2D resistivity data for imaging faults. *Journal of Applied Geophysics*, *57*(4), 260–277. https://doi.org/10.1016/j.jappgeo.2005.02.001

Nicollin, F., Gibert, D., Beauducel, F., Boudon, G., & Komorowski, J. C. (2006). Electrical tomography of La Soufrière of Guadeloupe Volcano: Field experiments, 1D inversion and qualitative interpretation. *Earth and Planetary Science Letters*, *244*(3–4), 709–724. https://doi.org/10.1016/j.epsl.2006.02.020

Orsi, G., Di Vito, M. A., & Isaia, R. (2004). Volcanic hazard assessment at the restless Campi Flegrei caldera. *Bulletin of Volcanology*, *66*(6), 514–530. https://doi.org/10.1007/s00445-003-0336-4

Padron, E., Hernàndez, P. A., Pérez, N. M., Toulkeridis, T., Melián, G., Barrancos, J., et al. (2012). Fumarole/plume and diffuse CO_2 emission from Sierra Negra caldera, Galapagos archipelago. *Bulletin of Volcanology*, *74*(6), 1509–1519. https://doi.org/10.1007/s00445-012-0610-4

Pepe, S., De Siena, L., Barone, A., Castaldo, R., D'Auria, L., Manzo, M., et al. (2019). Volcanic structures investigation through SAR and seismic interferometric methods: The 2011–2013 Campi Flegrei unrest episode. *Remote Sensing of Environment*, *234*, 111440. https://doi.org/10.1016/j.rse.2019.111440

Revil, A., Johnson, T. C., & Finizola, A. (2010). Three-dimensional resistivity tomography of Vulcan's forge, Vulcano Island, Southern Italy. *Geophysical Research Letters*, *37*(15). https://doi.org/10.1029/2010GL043983

Rizzo, E., & Giampaolo, V. (2018). New deep electrical resistivity tomography in the High Agri Valley basin (Basilicata, Southern Italy). *Geomatics, Natural Hazards and Risk*, *10*(1), 197–218. https://doi.org/10.1080/19475705.2018.1520150

Rosas-Carbajal, M., Komorowski, J. C., Nicollin, F., & Gibert, D. (2016). Volcano electrical tomography unveils edifice collapse hazard linked to hydrothermal system structure and dynamics. *Scientific Reports*, *6*(1), 1–11. https://doi.org/10.1038/srep29899

Rosi, M., & Sbrana, A. (1987). The Phlegraeanfields: CNR Quad. de "La ricerca Scientifica (pp. 1–175).

Sabbarese, C., Ambrosino, F., Chiodini, G., Giudicepietro, F., Macedonio, G., Caliro, S., et al. (2020). Continuous radon monitoring during seven years of volcanic unrest at Campi Flegrei caldera (Italy). *Scientific Reports*, *10*(1), 9551. https://doi.org/10.1038/s41598-020-66590-w

Sapia, V., Villani, F., Fischanger, F., Lupi, M., Baccheschi, P., Pantosti, D., et al. (2021). 3-D deep electrical resistivity tomography of the major basin related to the 2016 Mw 6.5 Central Italy earthquake fault. *Tectonics*, *40*(4), e2020TC006628. https://doi.org/10.1029/2020TC006628

Sauret, E. S. G., Beaujean, J., Nguyen, F., Wildemeersch, S., & Brouyere, S. (2015). Characterization of superficial deposits using electrical resistivity tomography (ERT) and horizontal-to-vertical spectral ratio (HVSR) geophysical methods: A case study. *Journal of Applied Geophysics*, *121*, 140–148. https://doi.org/10.1016/j.jappgeo.2015.07.012

Siniscalchi, A., Tripaldi, S., Romano, G., Chiodini, G., Improta, L., Petrillo, Z., et al. (2019). Reservoir structure and hydraulic properties of the Campi Flegrei geothermal system inferred by audiomagnetotelluric, geochemical, and seismicity study. *Journal of Geophysical Research: Solid Earth*, *124*(6), 5336–5356. https://doi.org/10.1029/2018JB016514

Smith, V. C., Isaia, R., & Pearce, N. J. G. (2011). Tephrostratigraphy and glass compositions of post-15 kyr Campi Flegrei eruptions: Implications for eruption history and chronostratigraphic markers. *Quaternary Science Reviews*, *30*(25–26), 3638–3660. https://doi.org/10.1016/j.quascirev.2011.07.012

Stock, M. J., Humphreys, M. C. S., Smith, V. C., Isaia, R., Brooker, R. A., & Pyle, D. M. (2018). Tracking volatile behaviour in sub-volcanic plumbing systems using apatite and glass: Insights into pre-eruptive processes at Campi Flegrei, Italy. *Journal of Petrology*, *59*(12), 2463–2492. https://doi.org/10.1093/petrology/egy020

Stock, M. J., Humphreys, M. C. S., Smith, V. C., Isaia, R., & Pyle, D. M. (2016). Late-stage volatile saturation as a potential trigger for explosive volcanic eruptions. *Nature Geoscience*, *9*(3), 249–254. https://doi.org/10.1038/NGEO2639

Suski, B., Brocard, G., Authemayou, C., Muralles, B. C., Teyssier, C., & Holliger, K. (2010). Localization and characterization of an active fault in an urbanized area in central Guatemala by means of geoelectrical imaging. *Tectonophysics*, *480*(1–4), 88–98. https://doi.org/10.1016/j.tecto.2009.09.028

Tarchini, L., Ranaldi, M., Carapezza, M. L., Di Giuseppe, M. G., Isaia, R., Lucchetti, C., et al. (2019). Multidisciplinary studies of diffuse soil CO2 flux, gas permeability, self-potential, soil temperature highlight the structural architecture of Fondi di Baia craters (Campi Flegrei caldera, Italy). *Annals of Geophysics*, *61*. https://doi.org/10.4401/ag-7683

Tonarini, S., D'Antonio, M., Di Vito, M. A., Orsi, G., & Carandente, A. (2009). Geochemical and B–Sr–Nd isotopic evidence for mingling and mixing processes in the magmatic system that fed the Astroni volcano (4.1–3.8 ka) within the Campi Flegrei caldera (Southern Italy). *Lithos*, *107*(3–4), 135–151. https://doi.org/10.1016/j.lithos.2008.09.012

Troiano, A., Di Giuseppe, M. G., Patella, D., Troise, C., & De Natale, G. (2014). Electromagnetic outline of the Solfatara-Pisciarelli hydrothermal system, Campi Flegrei (Southern Italy). *Journal of Volcanology and Geothermal Research*, *277*, 9–21. https://doi.org/10.1016/j.jvolgeores.2014.03.005

Troiano, A., Di Giuseppe, M. G., Petrillo, Z., & Patella, D. (2009). Imaging 2D structures by the CSAMT method: Application to the Pantano di S. Gregorio Magno faulted basin (Southern Italy). *Journal of Geophysics and Engineering*, *6*(2), 120–130. https://doi.org/10.1088/1742-2132/6/2/003

Troiano, A., Isaia, R., Di Giuseppe, M. G., Tramparulo, F. D. A., & Vitale, S. (2019). Deep electrical resistivity tomography for a 3D picture of the most active sector of Campi Flegrei caldera. *Scientific Reports*, *9*(1), 15124. https://doi.org/10.1038/s41598-019-51568-0

Troiano, A., Isaia, R., Tramparulo, F. D. A., & Di Giuseppe, M. G. (2021). The Pisciarelli main fumarole mechanisms reconstructed by electrical resistivity and induced polarization imaging. *Scientific Reports*, *11*(1), 18639. https://doi.org/10.1038/s41598-021-97413-1

Troiano, A., Petrillo, Z., Di Giuseppe, M. G., Balasco, M., Diaferia, I., Di Fiore, B., et al. (2008). About the shallow resistivity structure of Vesuvius volcano. *Annals of Geophysics*, *51*(1), 181–189. https://doi.org/10.4401/ag-3043

Van Hoorde, M., Hermans, T., Dumont, G., & Nguyen, F. (2017). 3D electrical resistivity tomography of karstified formations using cross-line measurements. *Engineering Geology*, *220*, 123–132. https://doi.org/10.1016/j.enggeo.2017.01.028

Vargemezis, G. (2014). 3D geoelectrical model of geothermal spring mechanism derived from VLF measurements: A case study from Aggistro (Northern Greece). *Geothermics*, *51*, 1–8. https://doi.org/10.1016/j.geothermics.2013.09.001

Vitale, S., & Isaia, R. (2014). Fractures and faults in volcanic rocks (Campi Flegrei, Southern Italy): Insights into volcano tectonic processes. *International Journal of Earth Sciences*, *103*(3), 801–819. https://doi.org/10.1007/s00531-013-0979-0

Vitale, S., Isaia, R., Ciarcia, S., Di Giuseppe, M. G., Iannuzzi, E., Prinzi, E. P., et al. (2019). Seismically induced soft-sediment deformation phenomena during the volcano-tectonic activity of Campi Flegrei caldera (Southern Italy) in the last 15 kyr. *Tectonics*, *38*(6), 1999–2018. https://doi.org/10.1029/2018TC005267

Ward, S. H. (1990). *Geotechnical an environmental geophysics: Volume I: Review and tutorial*. Society of Exploration Geophysicists.

Yeh, H. F., Lin, H. I., Wu, C. S., Hsu, K. C., Lee, J. W., & Lee, C. H. (2015). Electrical resistivity tomography applied to groundwater aquifer at downstream of Chih-Ben Creek basin, Taiwan. *Environmental Earth Sciences*, *73*(8), 4681–4687. https://doi.org/10.1007/s12665-014-3752-1

Young, N., Isaia, R., & Gottsmann, J. (2020). Gravimetric constraints on the hydrothermal system of the Campi Flegrei caldera. *Journal of Geophysical Research: Solid Earth*, *125*(7), e2019JB019231. https://doi.org/10.1029/2019jb019231